IEEE Open Access Journal of
Power and Energy

Received 23 September 2020; revised 2 January 2021; accepted 24 January 2021.
Date of publication 2 February 2021; date of current version 10 February 2021.

Digital Object Identifier 10.1109/OAJPE.2021.3056507

Distributed Secondary Control of a Microgrid With A Generalized PI Finite-Time Controller

YUANSHI ZHANG[1] (Student Member, IEEE),
AMIN MOHAMMADPOUR SHOTORBANI[1,2] (Member, IEEE),
LIWEI WANG[1] (Member, IEEE), AND
BEHNAM MOHAMMADI-IVATLOO[2] (Senior Member, IEEE)

[1]School of Engineering, The University of British Columbia Okanagan, Kelowna, BC V1V 1V7, Canada
[2]Faculty of Electrical and Computer Engineering, University of Tabriz, Tabriz 56617, Iran

CORRESPONDING AUTHOR: A. MOHAMMADPOUR SHOTORBANI (a.m.shotorbani@ubc.ca)

This work was supported in part by the Natural Sciences and Engineering Research Council of Canada and in part by the Research Office of the University of Tabriz.

ABSTRACT This paper proposes a novel distributed secondary controller for droop-controlled microgrids to regulate the frequency and voltage, and autonomously share the power mismatch. The proposed scheme is entitled generalized proportional-intergal finite-time controller (GPI-FTC). The proposed GPI-FTC is synthesized based on the control Lyapunov function method and modifying the conventional PI controller by adding a consensus term to the integrand dynamic. The proposed distributed GPI-FTC provides plug-n-play capability, scalability, and fast finite-time convergence of the system states. Moreover, a reactive power sharing (Q-sharing) method is designed to improve the sharing pattern of reactive power under exact voltage regulation. Also, a distributed voltage observer is developed for average voltage regulation. Performance of the proposed GPI-FTC is validated through numerical simulations of the detailed model of the microgrid, including small signal analysis, load change, DG outage, Q-sharing, and performance comparison.

INDEX TERMS Distributed secondary control, finite-time control, microgrids, generalized PI controller.

I. INTRODUCTION

THE concept of microgrid was proposed to integrate distributed generations (DGs) efficiently and reliably [1]. A microgrid can operate autonomously in islanded mode subsequent to a contingency or at a designed schedule. As the islanded mode has lower equivalent inertia compared to the grid-connected mode, additional control loops are required to maintain the stability of the microgrid when interfacing high penetration of power-electronically DGs.

In control hierarchy of a microgrid, the primary layer is the droop control whereas the second layer corresponds to compensate the voltage and freuqancy deviations caused by the droop control [2]–[4]. The second layer can be implemented in different architectures [5]. Despite the fact that centralized architectures can provide certain advantages such as optimized grid operations, the communication failure can lower the reliability and cause instability. On the other hand, the decentralized control strategy may not handle all the control targets effectively owing to lack of communication [6]. In distributed control, in contrast, the control actions of each DG are determined by local measurements and information exchanged with neighbor DGs. A microgrid distributed secondary control (MDSC) can be designed using different policies with and without communication needs, including averaging and consensus methods, containment pinning consensus, and decentralized event-triggered control [5].

Recently, multi-agent systems (MAS)-based methods have been extensively employed in design of MDCSs [6]–[11]. A MDSC was proposed in [7] for islanded microgrids, in which the communications among DGs and loads are crucial for power balance. Besides, whenever variations are made on the configuration of the CN, the control law needs to be redesigned. Furthermore, the stability of the microgrid will be degraded significantly, if the DG in voltage/frequency mode fails. In [8] and [9], the frequency of each DG was controlled internally using the global data from the global positioning system (GPS). The local controllers were designed based on the global model of the microgrid. However, this method requires global data for stable operation, and demands complex calculations for scalability, i.e. plug-n-play capability of the DGs.

In [10], a distributed frequency control was introduced considering the communication constraints, and power mismatch of the microgrid was estimated employing the average consensus method. A cooperative MDSC was designed in [11], using the input-output feedback linearization method to restore the voltage subsequent to unprepared disturbances. However, the voltage and frequency regulation have not been discussed in [10] and [11], respectively.

A consensus-based proportional-integral (PI) controller with asymptotic convergence was proposed in [12] with an event-triggered exchange of data. A frequency MDSC was designed in [13] using a ratio-consensus algorithm, in which the output active power of each DG was updated proportional to the difference between the maximum and the minimum power output of the DGs [13]. In [14], a near-optimal consensus-based MDSC was designed and a linear quadratic regulator was developed for the secondary voltage regulation, considering the communication topology. However, the frequency control and active power sharing were ignored.

Although the averaging consensus method is broadly applied to the MDSC, the system balance might be disrupted until the consensus is converged [15]. A MDSC with dynamic weighted gains was developed in [15] to improve the results of the averaging method and maintain the load-supply balance during the convergence of the consensus algorithm.

Moreover, the consensus-based PI control [12], ratio consensus frequency control [13], the MDSC with dynamic weights [15], discrete-time MDSC [16], and the adaptive MDSC with feedback linearization [17] yield asymptotic convergence of the system states, which is slower than the convergence in finite-time controllers (FTCs).

The authors in [6] have summarize and compared the finite- and fixed-time distributed control strategies. To accelerate the synchronization of frequency loop of the MDSC, a FTC was proposed in [18]. Operating between two boundaries with the discontinuous sign function, the controller may give rise to chattering and thus destabilize the microgrid. In [19], a frequency FTC was designed based on the input-output partial feedback linearizing stabilization scheme, but the reactive power control loop is ignored. In [20], a distributed fixed-time secondary control was proposed to regulate the frequency and share active power in islanded microgrids with mobile emergency resources. However, the voltage regulation and reactive power sharing (Q-sharing) were overlooked. A finite-time MDSC was proposed in [21] to separate the convergence of voltage and frequency control loops. Moreover, control inputs were bounded by saturation constraints for practical applications. The hard switching sign function and a fractional power integrator were employed together to construct FTCs so that frequency regulation and power sharing could be realized simultaneously [21]. But, they may suffer from the chattering phenamona, which can cause instability. Finite-time MDSCs with proportional and terminal sliding mode control schemes were synthesized and continuous approximations of the designed FTCs were developed to eliminate chattering in [22] and [23] respectively. A frequency and active power sharing FTC was designed in [24] by applying feedback linearization method and the super-twisting control was employed to solve the chattering problem. However, its stability is conservative on the control gain and has to limit the gains regarding the communication weights. In [25], an optimal FTC with proportional scheme was proposed for the frequency loop whereas an asymptotic controller was used for the voltage loop to separate their convergence speeds. In [26], a PI-shaped sliding mode FTC was developed for frequency regulation, whereas the conventional P-shaped control was used for the active power control loop.

This paper proposes a generalized PI-FTC (GPI-FTC) built on the conventional PI scheme for MDSC, which is the generalized form of proportional and PI controllers. The proposed GPI-FTC is synthesized by adding a distributed consensus dynamic at the integrand, and is designed using the control Lyapunov function algorithm. Its Lyapunov stability and finite-time convergence are mathematically proven. The main contributions of this work are summarized as

- A generalized formulation of distributed control scheme is designed that includes all conventional proportional and PI control schemes with and without finite-time convergence. The proposed PI-shaped generalized secondary restoration finite-time controller provides more degrees of freedom for improvement of the transient responses of the control loops.
- The proposed GPI-FTC provides finite-time convergence and improves the transient response and the settling time, compared to the conventional controllers by adding the proposed consensus-based integrand terms to its dynamics.
- The proposed GPI-FTC with leader-following voltage regulation improves the Q-sharing scheme compared to the common leader-following methods and assimilate the Q-sharing pattern similar to the share of reactive powers under average-voltage regulation control.
- A distributed averaging observer with finite-time convergence is proposed for average-voltage estimation, which is employed in the proposed GPI-FTC with the average-voltage regulation scheme.

In the proposed distributed GPI-FTC, each DG uses local measurements and a sparse communication network to receive neighbors' information in order to achieve frequency control, voltage regulation, and power sharing. Therefore, the distributed architecture enables scalablity with plug-n-play functionality, robustness to DG outage, flexibility to the changes in topology of the communication network (CN), and model-free controllability without a need for the knowledge about microgrid's topology.

II. DROOP CONTROL AND GRAPH THEORY PRELIMINARIES

Figure 1 illustrates the hierarchical control architecture for an islanded microgrid. The DG output voltage and frequency

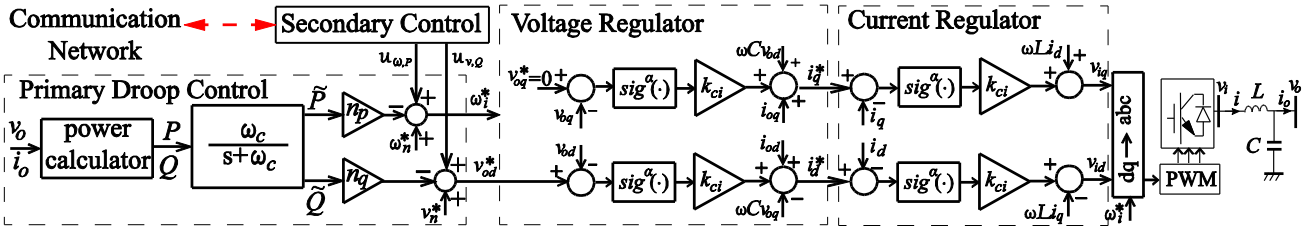

FIGURE 1. **Hierarchical control scheme diagram of the power-electronic converters with LC output filters in a droop-controller islanded microgrid.**

(i.e. v_{di} and ω_i) are determined by the primary control level. The droop control scheme is usually adopted in the primary layer to share the power mismatch automatically among the DGs. The major drawback of droop control in a microgrid is the resulted deviations of voltage and frequency from their nominal referneces [26]. Moreover, the impact of line impedance greatly influences the accuracy of Q-sharing in voltage droop control [27]. Therefore, the secondary control layer is adopted to mitigate the deviations and improve the Q-sharing. The secondary control signal is added to the voltage and frequency reference of the primary droop control as a supplementary control signal. The inner voltage and current regulators of the converters are designed using FTCs as shown in Fig. 1.

The droop control for the primary level is modeled as

$$\omega_i = u_{\omega,Pi} + \omega_n^* - n_{Pi}\tilde{\mathbf{P}}_i \tag{1}$$

$$\begin{cases} v_{od,i} = |V|_i = u_{v,Qi} + V_n^* - n_{Qi}\tilde{Q}_i \\ v_{oq,i} = 0 \end{cases} \tag{2}$$

where $|V|_i$ is the voltage magnitude of the i^{th} DG; ω_i is the frequency;V_n^* and ω_n^* are the nominal voltage and frequency; $v_{od,i}$ and $v_{oq,i}$ are the d- and q- axis components of the i^{th} DG voltage; $u_{\omega,Pi}$ and $u_{v,Qi}$ are the frequency and voltage supplementary control signals produced by the secondary control level; n_{Pi} and n_{Qi} are the droop coefficients; and

$$\tilde{\mathbf{P}}_i = \frac{\omega_c}{s+\omega_c}P_i, \quad \tilde{Q}_i = \frac{\omega_c}{s+\omega_c}Q_i \tag{3}$$

where ω_c is the cut-off frequency of the low-pass filter [9]; P_i and Q_i are the output active and reactive powers.

The CN can be represented as a digraph $G(\mathcal{V}, \boldsymbol{\varepsilon}, \mathcal{A})$, where $\mathcal{V}$ is the nodes set; $\boldsymbol{\varepsilon} \subseteq \mathcal{V}\times\mathcal{V}$ is the edges set; and $\mathcal{A} = [a_{ij}]$ is the adjacency matrix. The CN links and the DGs conform the edges and the vertices of the CN graph G, respectively. The neighbor set of node i is defined as $N_i = \{j | (V_i, V_j) \in \boldsymbol{\varepsilon}\}$. The Laplacian matrix of G is calculated as $\mathbf{L} = \mathbf{D} - \mathcal{A}$, where $\mathbf{D}$ is the in-degree matrix of G. We define $\mathbf{G} = \text{diag}(g_i)$ as the pinning matrix, where $g_i \geq 0$ is the weight of the edge between the i^{th} DG and the virtual leader [28], and $\boldsymbol{\Gamma} = \mathbf{L}+\mathbf{G}$.

III. PROPOSED DISTRIBUTED SECONDARY GPI-FTC

In order to regulate the voltage and frequency of the droop controlled microgrid and preserve the droop-based power-sharing pattern, the proposed secondary GPI-FTC is designed based on the proportional-integral control scheme using the control Lyapunov function method, by adding a new consensus-based term to the integrand taking the integrands of the neighboring units into consideration. Finite-time convergence and stability of the proposed GPI-FTCs are proved using the Lyapunov stability criteria.

A. PROPOSED PI FREQUENCY AND POWER-SHARING CONTROLLERS

The frequency and the active power-sharing errors are defined as [29]:

$$e_{\omega i} = g_i\left(\omega_i - \omega_n^*\right) + \sum\nolimits_{j\in N_i} a_{ij}\left(\omega_i - \omega_j\right) \tag{4}$$

$$e_{Pi} = \sum\nolimits_{j\in N_i} a_{ij}\left(n_{Pi}\tilde{\mathbf{P}}_i - n_{Pj}\tilde{\mathbf{P}}_j\right) \tag{5}$$

The supplementary secondary control signal to regulate frequency and the active power is given as:

$$u_{\omega,Pi} = \int (u_{\omega i} + u_{Pi})\, dt \tag{6}$$

which includes two distinct controllers for frequency regulation (i.e. $u_{\omega i}$) and active power-sharing (i.e. u_{Pi}).

The proposed frequency controller is designed as

$$\begin{cases} u_{\omega,i} = -k_{\omega,i}^P \text{sig}^\alpha\left(e_{\omega,i}\right) - k_{\omega,i}^I \text{sig}^\alpha\left(z_{\omega,i}\right) \\ \dot{z}_{\omega,i} = \text{sig}^\alpha\left(e_{\omega,i}\right) - k_{\omega,i}^Z \sum_{j\in N_i} a_{ij}(\text{sig}^\alpha\left(z_{\omega,i}\right) - \text{sig}^\alpha\left(z_{\omega,j}\right)) \end{cases} \tag{7}$$

where $z_{\omega,i}$ is the integrand; $k_{\omega,i}^P > 0$ is the proportional gain; $k_{\omega,i}^I > 0$ is the integral gain; $k_{\omega,i}^Z > 0$ is the integrand gain; $\text{sig}^\alpha\left(e_{\omega,i}\right) = \left|e_{\omega,i}\right|^\alpha \text{sgn}\left(e_{\omega,i}\right)$; $\text{sgn}(\bullet)$ is the sign function; $0 < \alpha < 1$ is the fractional power of the finite-time terms.

The proposed power-sharing controller of the frequency and the active power-sharing is designed as

$$\begin{cases} u_{P,i} = -k_{P,i}^P \text{sig}^\alpha(e_{P,i}) - k_{P,i}^I \text{sig}^\alpha(z_{P,i}) \\ \dot{z}_{P,i} = \text{sig}^\alpha(e_{P,i}) - k_{P,i}^Z \sum_{j\in N_i} a_{ij}(\text{sig}^\alpha\left(z_{P,i}\right) - \text{sig}^\alpha\left(z_{P,j}\right)) \end{cases} \tag{8}$$

where $z_{P,i}$ is the integrand; $k_{P,i}^P > 0$ is the proportional gain; $k_{P,i}^I > 0$ is the integral gain; and $k_{P,i}^Z > 0$ is the integrand gain.

B. VOLTAGE REGULATION WITH COOPERATIVE SECONDARY GPI-FTC

Similarly, the voltage and the reactive power-sharing errors can be defined as [29]:

$$e_{vi} = g_i\left(v_i - v_n^*\right) + \sum\nolimits_{j\in N_i} a_{ij}\left(v_i - v_j\right) \tag{9}$$

$$e_{Qi} = \sum\nolimits_{j\in N_i} a_{ij}\left(n_{Qi}\tilde{Q}_i - n_{Qj}\tilde{Q}_j\right) \tag{10}$$

The supplementary secondary control signal to regulate voltage and reactive power is given as:

$$u_{v,Qi} = \int \left(u_{vi} + u_{Qi}\right) dt \tag{11}$$

which includes two distinct controllers for frequency regulation (i.e. u_{vi}) and power-sharing (i.e. u_{Qi}) respectively.

The proposed voltage controller is designed as

$$\begin{cases} u_{v,i} = -k_{v,i}^P \mathrm{sig}^\alpha\left(e_{v,i}\right) - k_{v,i}^I \mathrm{sig}^\alpha\left(z_{v,i}\right) \\ \dot{z}_{v,i} = \mathrm{sig}^\alpha\left(e_{v,i}\right) - k_{v,i}^Z \sum_{j\in N_i} a_{ij}(\mathrm{sig}^\alpha\left(z_{v,i}\right) - \mathrm{sig}^\alpha\left(z_{v,j}\right)) \end{cases} \tag{12}$$

where $z_{v,i}$ is the integrand; $k_{v,i}^P > 0$ is the proportional gain; $k_{v,i}^I > 0$ is the integral gain; and $k_{v,i}^Z > 0$ is the integrand gain;

The proposed Q-controller is designed as

$$\begin{cases} u_{Q,i} = -k_{Q,i}^P \mathrm{sig}^\alpha\left(e_{Q,i}\right) - k_{Q,i}^I \mathrm{sig}^\alpha\left(z_{Q,i}\right) \\ \dot{z}_{Q,i} = \mathrm{sig}^\alpha\left(e_{Q,i}\right) - k_{Q,i}^Z \sum_{j\in N_i} a_{ij}(\mathrm{sig}^\alpha\left(z_{Q,i}\right) - \mathrm{sig}^\alpha\left(z_{Q,j}\right)) \end{cases} \tag{13}$$

where $z_{Q,i}$ is the integrand; $k_{Q,i}^P > 0$ is the proportional gain; $k_{Q,i}^I > 0$ is the integral gain; and $k_{Q,i}^Z > 0$ is the integrand gain.

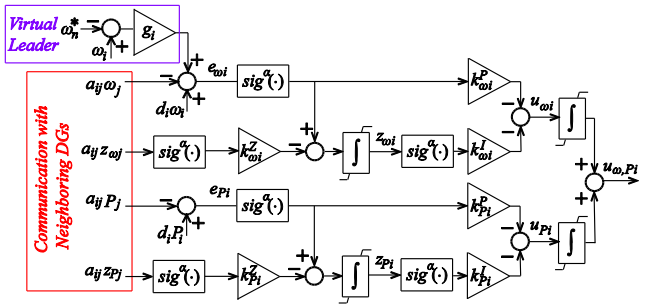

FIGURE 2. Schematic diagram of the proposed GPI-FTC for frequency regulation and P-sharing control.

Fig. 2 illustrates the diagram of the supplementary control signal for the proposed GPI-FTC, which is added to the droop control level as shown in (1) and (2). Fig. 2 shows how to produce the supplementary control signal to regulate the frequency and active power-sharing according to (6), (7) and (8). The supplementary GPI-FTC signal to regulate the voltage and the reactive power based on (11), (12) and (13) are generated similarly.

Proposition 1: The proposed GPI-FTC regulates the drooped frequency of the microgrid to the nominal value and automatically shares the active power demand between the DGs. As a result, at the steady state, the system converges to:

$$\lim_{t\to\infty} \omega_i\left(t\right) = \omega_n^* \tag{14}$$

$$\forall i,j: \lim_{t\to\infty} n_{Pi}P_i\left(t\right) = \lim_{t\to\infty} n_{Pj}P_j\left(t\right) \tag{15}$$

where ω_n^* is the reference frequency.

Proposition 2: Similarly, the proposed GPI-FTC regulates the voltage to the nominal value and automatically shares the reactive power demand between the DGs.

Exact voltage regulation and Q-sharing are two conflicting objectives. Instead, average voltage regulation has been applied using consensus methods [28] to provide an accurate Q-sharing and to account for the effect of the line impedances. A compromise between the exact voltage regulation and Q–sharing control is established in the proposed controller instead of average voltage regulation. This is because the latter is already widely addressed in the studies such as [16], [21], [28]. Clearly, exact Q-sharing is not feasible due to the impacts of line impedances. However, the proposed Q-sharing controller reduces the Q-sharing error compared to exact regulation of the voltage.

In addition to exact voltage regulation and the proposed voltage regulation with Q-sharing control, the proposed scheme can be employed for average-voltage regulation by utilizing a distributed observer to locally estimate the average voltage of the microgrid. A distributed finite-time average consensus observer is proposed using a similar approach for the distributed consensus observer in [30]. The dynamic of the proposed distributed average observer is designed as

$$\hat{\boldsymbol{\varphi}}_{di} = \frac{1}{1+d_i}\left[v_{di} + \mu_i \int \mathrm{sig}^\gamma\left(v_{di} - \hat{\boldsymbol{\varphi}}_{di}\right) dt + \sum_{j\in N_i} a_{ij}\hat{\boldsymbol{\varphi}}_{dj} - \mu_i \int \mathrm{sig}^\gamma\left(\sum_{j\in N_i} a_{ij}\left(\hat{\boldsymbol{\varphi}}_{di} - \hat{\boldsymbol{\varphi}}_{dj}\right)\right) dt\right] \tag{16}$$

where $\hat{\boldsymbol{\varphi}}_{di}$ is the estimation of the average voltage at the i^{th} DG, $\mu_i > 0$ is a constant gain, and $0 < \gamma < 1$ is the fractional power. Schematic diagram of the proposed distributed avergae voltage observer is shown in Fig. 3.

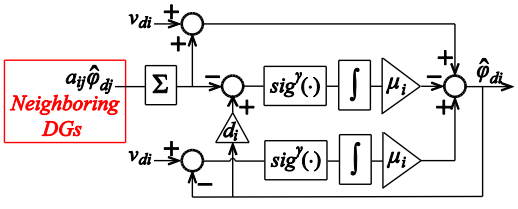

FIGURE 3. Distributed average voltage observer diagram.

The proposed distributed observer (16) estimates the average voltage of the DG busses, with finite-time convergence characteristic, i.e.:

$$\lim_{t\to T_s} \hat{\boldsymbol{\varphi}}_{di}\left(t\right) \to \bar{v}_d = \frac{1}{n}\sum\nolimits_{i=1}^{n} v_{di}\left(t\right) \tag{17}$$

where T_s is the finite settling time, which is bounded as (20)

$$T_s \leq \frac{1}{\mu\left(1-\gamma\right)}\sum_i\left(\left|\hat{\boldsymbol{\varphi}}_{di}\left(0\right)-\frac{1}{n}\sum_i v_{di}\left(0\right)\right|^{1-\gamma}+\left|d_i\hat{\boldsymbol{\varphi}}_{di}\left(0\right)-\sum_{j\in N_i}a_{ij}\hat{\boldsymbol{\varphi}}_{dj}\left(0\right)\right|^{1-\gamma}\right) \quad (18)$$

where $\mu=\min\{\mu_i\}$, $\hat{\boldsymbol{\varphi}}_{di}\left(0\right)$ is the initial estimation in i^{th} DG at $t=0$, and $v_{di}\left(0\right)$ is the i^{th} DG voltage at $t=0$.

Proposition 3: The average-voltage regulation can be achieved by utilizing the proposed voltage and Q-sharing controllers (12) and (13), and employing the proposed distributed observer (16) to locally estimate the average voltage of the DGs, and by redefining the voltage error (9) only at the virtual leaders as:

$$e_{vi}=g_i\left(\hat{\boldsymbol{\varphi}}_{di}-v_n^*\right)+\sum\nolimits_{j\in\hat{\mathrm{E}}N_i}a_{ij}\left(v_{d,i}-v_{d,j}\right) \quad (19)$$

which in vector form is written as

$$\mathbf{e}_{\boldsymbol{\mathcal{V}}}=[e_{vi}]=\mathbf{L}\mathbf{v}+\mathbf{G}\left(\hat{\boldsymbol{\varphi}}_d-\boldsymbol{\mathcal{V}}_n^*\right) \quad (20)$$

where $\hat{\boldsymbol{\varphi}}_d=\left[\hat{\boldsymbol{\varphi}}_{di}\right]$.

C. LYAPUNOV STABILITY AND FINITE-TIME CONVERGENCE OF THE PROPOSED CONTROLLERS

Stability of the microgrid control loops under the proposed GPI-FTC is proved using the Lyapunov stability criteria. In the following, the stability of the proposed *P*-sharing controller is proved as an instance. The stability of the proposed frequency and voltage controllers as well as the proposed Q-sharing controller can be proved in an identical approach, which is not included for brevity.

From (4)–(8), the errors and controllers in vector form are:

$$\mathbf{e}_{\boldsymbol{\omega}}=[e_{\omega i}]=\mathbf{G}\left(\boldsymbol{\omega}-\boldsymbol{\omega}_n^*\right)+\mathbf{L}\omega \quad (21)$$

$$\mathbf{e}_{\mathbf{P}}=[e_{Pi}]=\mathbf{L}\mathbf{n}_{\mathbf{P}}\tilde{\mathbf{P}} \quad (22)$$

$$\dot{\mathbf{u}}_{\omega,P}=\mathbf{u}_{\boldsymbol{\omega}}+\mathbf{u}_{\mathbf{P}} \quad (23)$$

$$\begin{cases}\mathbf{u}_\omega=\left[\psi_{\omega,i}\right]=-\mathbf{K}_\omega^P\mathrm{sig}^\alpha\left(\mathbf{e}_\omega\right)-\mathbf{K}_\omega^I\mathrm{sig}^\alpha\left(\mathbf{z}_\omega\right)\\ \dot{z}_\omega=\left[\dot{z}_{\omega,i}\right]=\mathrm{sig}^\alpha\left(\mathbf{e}_\omega\right)-\mathbf{K}_\omega^Z\mathbf{L}\mathrm{sig}^\alpha\left(\mathbf{z}_\omega\right)\end{cases} \quad (24)$$

$$\begin{cases}\mathbf{u}_P=\left[\psi_{P,i}\right]=-\mathbf{K}_P^P\mathrm{sig}^\alpha\left(\mathbf{e}_P\right)-\mathbf{K}_P^I\mathrm{sig}^\alpha\left(\mathbf{z}_\omega\right)\\ \dot{z}_P=\left[\dot{z}_{P,i}\right]=\mathrm{sig}^\alpha\left(\mathbf{e}_P\right)-\mathbf{K}_P^Z\mathbf{L}\mathrm{sig}^\alpha\left(\mathbf{z}_P\right)\end{cases} \quad (25)$$

where $\mathbf{K}_\omega^P=\mathrm{diag}\left(k_{\omega,i}^P\right)$, $\mathbf{K}_\omega^I=\mathrm{diag}\left(k_{\omega,i}^I\right)$, $\mathbf{K}_\omega^Z=\mathrm{diag}\left(k_{\omega,i}^Z\right)$, $\mathbf{K}_P^P=\mathrm{diag}\left(k_{P,i}^P\right)$, $\mathbf{K}_P^I=\mathrm{diag}\left(k_{P,i}^I\right)$, and $\mathbf{K}_P^Z=\mathrm{diag}\left(k_{P,i}^Z\right)$ are diagonal gain matrices.

Considering $\mathbf{n}_{\mathbf{P}}\tilde{\mathbf{P}}$ **in** (22) as the *P*-sharing controller [9], [29] (i.e. $\mathbf{u}_P=\mathbf{n}_{\mathbf{P}}\dot{\tilde{\mathbf{P}}}$) and (25), the power-sharing error dynamic is

$$\dot{e}_{\mathbf{P}}=\mathbf{L}\mathbf{n}_{\mathbf{P}}\dot{\tilde{\mathbf{P}}}=\mathbf{L}\mathbf{u}_P=-\mathbf{L}\mathbf{K}_P^P\mathrm{sig}^\alpha\left(\boldsymbol{\varepsilon}_P\right)-\mathbf{L}\mathbf{K}_P^I\mathrm{sig}^\alpha\left(\mathbf{z}_P\right) \quad (26)$$

Considering the state variables $\boldsymbol{\varepsilon}_{\mathbf{P}}$ and $\mathbf{z}_{\mathbf{P}}$, the closed-loop state-space model of the *P*-sharing control loop is derived as

$$\frac{d}{dt}\begin{pmatrix}\mathbf{e}_P\\ \mathbf{z}_P\end{pmatrix}=-\mathbf{A}_P\mathrm{sig}^\alpha\begin{pmatrix}\mathbf{e}_P\\ \mathbf{z}_P\end{pmatrix},\quad \mathbf{A}_P=\begin{pmatrix}\mathbf{K}_P^P\mathbf{L} & \mathbf{K}_P^I\mathbf{L}\\ -\mathbf{I} & \mathbf{K}_P^Z\mathbf{L}\end{pmatrix} \quad (27)$$

In the following, the mathematical proof for finite-time convergence of the active power-sharing control loop under the proposed GPI-FTC is discussed using the control Lyapunov function $V_P=\frac{1}{2}\boldsymbol{\varepsilon}_P^T\boldsymbol{\varepsilon}_P+\frac{1}{2}\mathbf{z}_P^T\mathbf{z}_P=\frac{1}{2}\sum_i e_{P,i}^2+\frac{1}{2}\sum_i z_{P,i}^2$ and by showing that $\frac{d}{dt}V_p\leq-cV_P^\beta$, whereat where $c>0$ and $0<\beta<1$ are real positive constants [19], [21], [22], [24], [26], [31]. The stability proof and finite-time convergence of the frequency, voltage, and reactive power loops under the proposed GPI-FTC have an identical approach.

Consider the Lyapunov function

$$V_P=\frac{1}{2}\mathbf{e}_P^T\mathbf{e}_P+\frac{1}{2}\mathbf{z}_P^T\mathbf{z}_P=\frac{1}{2}\sum\nolimits_i e_{P,i}^2+\frac{1}{2}\sum\nolimits_i z_{P,i}^2 \quad (28)$$

Substituting $\dot{e}_P$ from (26) and $\dot{z}_P$ from (15) into $\dot{V}_P=\mathbf{e}_P^T\dot{e}_P+\mathbf{z}_P^T\dot{z}_P$ yields

$$\dot{V}_P=\left(\mathbf{e}_P^T,\mathbf{z}_P^T\right)\begin{pmatrix}\dot{e}_P\\ \dot{z}_P\end{pmatrix}=-\left(\mathbf{e}_P^T,\mathbf{z}_P^T\right)\mathbf{A}_P\mathrm{sig}^\alpha\begin{pmatrix}\mathbf{e}_P\\ \mathbf{z}_P\end{pmatrix} \quad (29)$$

The system is Lyapunov-stable if the LMI $\mathbf{A}_P>0$ is satisfied. Suppose $\lambda_{\mathbf{A}_P}$ are the eigenvalues of $\mathbf{A}_P$; and $\lambda_{\mathbf{A}_P}^{\min}=\min\left\{\left|\Re\left(\lambda_{\mathbf{A}_P}\right)\right|\right\}$ is the minimum absolute real part of the eigenvalues $\lambda_{\mathbf{A}_P}$.

Consequently, it is concluded from (29) that:

$$\dot{V}_P\leq-\lambda_{\mathbf{A}_P}^{\min}\left(\mathbf{e}_P^T\mathrm{sig}^\alpha\left(\mathbf{e}_P\right)+\mathbf{z}_P^T\mathrm{sig}^\alpha\left(\mathbf{z}_P\right)\right) \quad (30)$$

and thus

$$\begin{aligned}\dot{V}_P&\leq-\lambda_{\mathbf{A}_P}^{\min}\sum\nolimits_i\left(\left|e_{P,i}\right|^{\alpha+1}+\left|z_{P,i}\right|^{\alpha+1}\right)\\&=-\lambda_{\mathbf{A}_P}^{\min}\sum\nolimits_i\left(\left(e_{P,i}^2\right)^\beta+\left(z_{P,i}^2\right)^\beta\right)\end{aligned} \quad (31)$$

where $0<\beta=\frac{\alpha+1}{2}<1$ is a real positive constant.

For $0<\beta<1$, we have:

$$\begin{aligned}\sum\nolimits_i\left(e_{P,i}^{2\beta}+z_{P,i}^{2\beta}\right)&\leq\sum\nolimits_i\left(e_{P,i}^2+z_{P,i}^2\right)^\beta\\&\leq\left(\sum\nolimits_i e_{P,i}^2+z_{P,i}^2\right)^\beta\end{aligned} \quad (32)$$

From (31) and (32), it is concluded that:

$$\dot{V}_P\leq-\lambda_{\mathbf{A}_P}^{\min}2^\beta\left(\frac{1}{2}\sum\nolimits_i e_{P,i}^2+z_{P,i}^2\right)^\beta\leq-2^\beta\lambda_{\mathbf{A}_P}^{\min}V_P^\beta \quad (33)$$

which confirms the Lyapunov stability and finite-time convergence [31] of the proposed power-sharing control loop. Consequently, the finite settling time of the control loop is:

$$t_s\leq\frac{\left(V_P\left(0\right)\right)^{1-\beta}}{2^\beta\lambda_{\mathbf{A}_P}^{\min}\left(1-\beta\right)}\leq\frac{\left(\left\|\mathbf{e}_P\left(0\right)\right\|+\left\|\mathbf{z}_P\left(0\right)\right\|\right)^{1-\alpha}}{\lambda_{\mathbf{A}_P}^{\min}\left(1-\alpha\right)} \quad (34)$$

The stability proof and finite-time convergenc of the frequency GPI-FTC has an identical approach, and is not included for briefness.

For the positive control gains and a connected CN, it is obvious that we have $\mathbf{A}_P \geq 0$ and thus $\lambda^{\min}_{\mathbf{A}_P} \geq 0$. Clearly, selecting positive control gains is sufficient for Lyapunov stability of the proposed control loops.

While the structure of CN can be altered, the stability of the control loops is preserved as long as the altered CN graph contains a spanning tree [16], [21], [29]. Therefore, establishing an intermittently connected CN is required for the stability of the control loops.

Regarding (34), the settling time of the control loop is inversely affected by the control gains. With respect to (27), (30) and (34), the active (reactive) power-sharing control gains can be designed so that $\lambda^{\min}_{\mathbf{A}_P} < \lambda^{\min}_{\mathbf{A}_\omega}$ ($\lambda^{\min}_{\mathbf{A}_Q} < \lambda^{\min}_{\mathbf{A}_v}$) and thus the settling time of the frequency (voltage) regulation loop be lower than the settling time of the active (reactive) power-sharing control loop.

D. COMPARISON WITH THE PROPORTIONAL- AND THE PI-SHAPED CONTROLLERS

The proposed GPI-FTC comprehensively includes the conventional proportional- and the PI-shaped control structures. A different PI-shaped scheme can be achieved by setting the integrand gain to zero (i.e. $k_i^Z = 0$) in the proposed GPI-FTC, which gives:

$$\begin{cases} \psi^{PI-FTC}_{\omega,i} = -k_i^P \mathrm{sig}^\alpha\left(e_{\omega,i}\right) - k^I_{\omega,i}\mathrm{sig}^\alpha\left(z_{\omega,i}\right) \\ \dot{z}^{PI-FTC}_{\omega,i} = \mathrm{sig}^\alpha\left(e_{\omega,i}\right) \end{cases} \tag{35}$$

The common structure of the PI-shaped FTC [19], [21], [26] can also be achieved by substituting $z_{\omega,i}$ for $\mathrm{sig}^\alpha\left(z_{\omega,i}\right)$ in (35) as

$$\begin{aligned} \psi^{PI_2-FTC}_{\omega,i} &= -k_i^P \mathrm{sig}^\alpha\left(e_{\omega,i}\right) - k^I_{\omega,i} z_{\omega,i} \\ &= -k_i^P \mathrm{sig}^\alpha\left(e_{\omega,i}\right) - k^I_{\omega,i}\int \mathrm{sig}^\alpha\left(e_{\omega,i}\right) dt \end{aligned} \tag{36}$$

Moreover, the common proportional FTC structure [22], [24] can be achieved by setting the integral and integrand gains to zero (i.e. $k_i^I = 0$ and $k_i^Z = 0$) in the proposed GPI-FTC, which gives:

$$\psi^{P-FTC}_{\omega,i} = -k_i^P \mathrm{sig}^\alpha\left(e_{\omega,i}\right) \tag{37}$$

Furthermore, the asymptotic-convergent controllers with the proportional [6], [16], [17], [29], [R1], [R2], and the PI-shaped [11], [12], [28], [R3], [R4] structure are achieved by setting the fractional power $\alpha = 1$ in (36) and (37) as

$$\psi^{PI-ACC}_{\omega,i} = -k_i^P e_{\omega,i} - k^I_{\omega,i}\int e_{\omega,i} dt \tag{38}$$

$$\psi^{P-ACC}_{\omega,i} = -k_i^P e_{\omega,i} \tag{39}$$

where the superscript *ACC* denotes the asymptotic convergence controller.

The proposed GPI-FTC provides finite-time convergence with a distinct structure compared to existing P-shaped [22], [24], and PI-shaped [19], [21], [26] controllers. Moreover, the designed scheme is less conservative on control parameters compared to the LMI conditions in [17], [21], [27]. The proposed controllers feature the leader-following schemes [16], [17], [21]. The reference voltage and frequency values are determined by the virtual leaders, which resembles a pinning control scheme [16], [21].

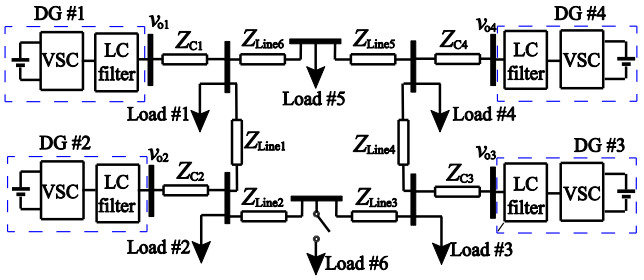

FIGURE 4. Schematic diagram of the power layer of the microgrid [26].

TABLE 1. Microgrid system parameters [19], [26].

Symbol	Description	Quantity
v_n^*, ω_n^*	Nominal voltage and frequency	380 V, 50 Hz
n_P, n_Q	Droop Gains of DG1&2	$9.4\times10^{-5}, 1.3\times10^{-3}$
n_P, n_Q	Droop Gains of DG3&4	$12.5\times10^{-5}, 1.5\times10^{-3}$
ω_c	Droop filter cut-off frequency	12π
R_f, L_f, C_f	RLC Filter Impedance	0.1 Ω, 1.35 mH, 47 μF
PI_v	Voltage regulator	$0.1 + 420/s$
PI_c	Current regulator	$15 + 20e3/s$
Z_{Ci}	Coupling Impedance	0.03+j1.31 Ω
$Z_{Line1,4,5}$	Distribution Line	0.12+j0.1 Ω
$Z_{Line2,3}$	Distribution Line	0.088+j0.29 Ω
Z_{Line6}	Distribution Line	0.175+j0.58 Ω
Load	Load #1: 300 Ω, 477 mH,	Load #2: 40 Ω, 64 mH
Load	Load #3: 50 Ω, 64 mH,	Load #4: 50 Ω, 95 mH
Load	Load #5: 20 Ω, 32 mH,	Load #6: 30 Ω, 47 mH

IV. CASE STUDIES

Fig. 4 shows the single-line power layer of a typical islanded microgrid, including 4 DGs and 5 loads originally (an additional load will be switched on in Case 2). The system parameters of the microgrid are given in Table 1 [26]. With the scheme shown in Fig.1 and detailed parameters listed in Table 1, the voltage and current regulators are employed to be the inner control loops of DGs. The microgrid, the CN, and the control loops are modeled in MATLAB/Simulink Simscape Electrical Blockset.

A continuous approximation of the sign function (i.e. $sign\,(x) = \tanh\,(cx)\,, c > 0$ is used to avoid chattering in the proposed FTC.

Numerical scenarios are studied to examine the performance of the proposed GPI-FTC, such as: I–Small signal analysis; II–Connection of a new load; III–Performance comparison of the proposed GPI-MDSC with the exact voltage regulation; and IV–A DG is forced outage. The

TABLE 2. Parameters of the proposed GPI-MDSC.

Symbol	Description	Quantity
$k^P_{\omega,i}, k^P_{P,i}, k^P_{v,i}, k^P_{Q,i}$	Proportional Gain of the GPI	15
$k^I_{\omega,i}, k^I_{P,i}, k^I_{v,i}, k^I_{Q,i}$	Integral Gain of the GPI	15
$k^Z_{\omega,i}, k^Z_{P,i}, k^Z_{v,i}, k^Z_{Q,i}$	Integrand Gain of the GPI	15

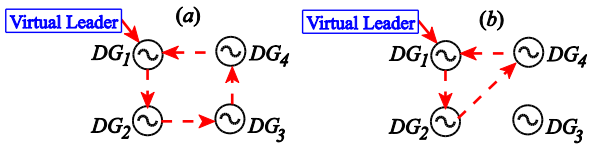

FIGURE 5. Illustrations of the CN topology: (a) Normal operation; (b) DG 3 outage.

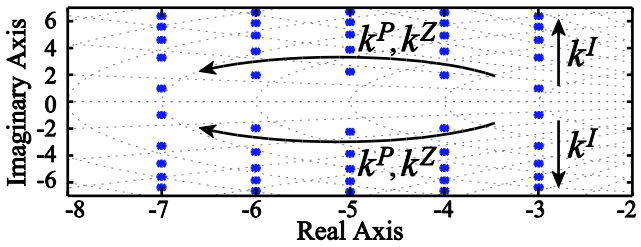

FIGURE 6. Impact of control gains on the dominant modes. The grid lines are shown at $\omega_n = 3, 4, 5, 6, 7$ and $\zeta = 0.34, 0.41, 0.48, 0.57, 0.68, 0.78, 0.88, 0.97$.

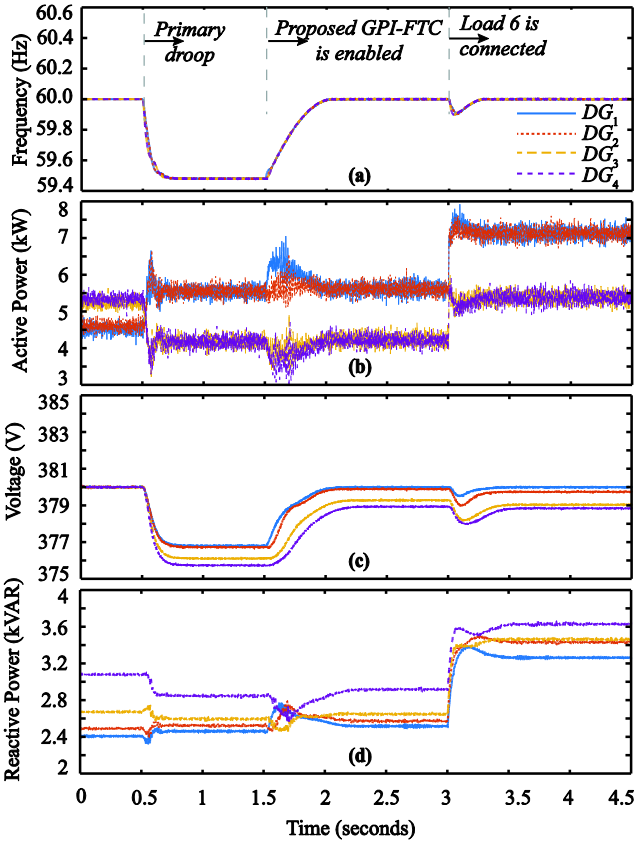

FIGURE 7. DG outputs when load increases: (a) Frequency; (b) Active Power; (c) Voltage; (d) Reactive power.

pinning gains are set to be $g_1 = 1$ and $g_2 = g_3 = g_4 = 0$ [19], [29] because it is assumed that only DG 1 has connection with the virtual leader.The CN topology shown in Fig. 5 (a) is utilized for all the cases except when DG 3 is forced outage in Case 3, whereas it is altered to Fig. 4 (b) after the outage of DG 3.

A. CASE 1. SMALL SIGNAL ANALYSIS

Fig. 6 depicts the trajectories of the dominant modes of the closed-loop system, when each control gain is increased from 1 to 10 while other gains are kept constant at 5. Dominant modes move away from the imaginary axis and toward the real axis by increasing k^Z (either k^Z_v and k^Z_ω) and k^P (either k^P_v and k^P_ω). The proposed GPI-FTC scheme provides higher degree of freedom in regulating the transient behavior [24] compared to proportional controller. The impact of k^Z in Fig. 6, implies that the proposed GPI-FTC yields larger closed-loop eigenvalues, compared to the conventional PI schemes [21], [26], [29] in which $k^Z_v = k^Z_\omega = 0$.

The conventional consensus-and-PI-based controller can also be improved by using the communication weights or coupling gain. However, the coupling gain resembles adding the consensus-based error to the proportional part of the PI controller. Adding the consensus-based error $\sum_{j\in N_i} a_{ij}(\text{sig}^\alpha(e_{\omega,i}) - \text{sig}^\alpha(e_{\omega,j}))$ is similar to modifying the proportional gain of the controller under the effect of the Laplacian matrix gains. However, modifying the communication weights or coupling gains can affect the performance and convergence of the consensus algorithm including the distributed average voltage observer. As shown in Fig. 6, adding the integrand-based consensus error $\sum_{j\in N_i} a_{ij}(\text{sig}^\alpha(z_{\omega,i}) - \text{sig}^\alpha(z_{\omega,j}))$ to the dynamics of the integrand in the proposed GPI-FTC can act identical to modifying the proportional control gain (i.e. $\mathbf{K}^P$) as the gains $\mathbf{K}^Z$ and $\mathbf{K}^P$ have similar impact on the dominant modes illustrated in Fig. 6. Nonetheless, the proposed method provides one more degree of freedom, and the control gains $\mathbf{K}^Z$ and $\mathbf{K}^P$ can be modified independently.

B. CASE 2. PERFORMANCE OF THE GPI-FTC WHEN LOAD CHANGES

In this case, the primary droop is activated at $t = 0.5s$. Then, the proposed GPI-MDSC is enabled at $t = 1.5s$. Moreover, the Load 6 is connected at $t = 3$. The output frequency, voltage, active power, and reactive powers of the DGs are shown in Fig. 7. As shown in Fig. 5 (a), the microgrid frequency deviates from its nominal value under the primary droop and without the secondary control. Enabling the proposed GPI-FTC restores the microgrid frequency and voltage to their nominal values and automatically shares the power demand among the DGs.

As shown in Figs. 7 (c) and (d), the leader-following voltage regulation (DG 1 is the leader) with the proposed

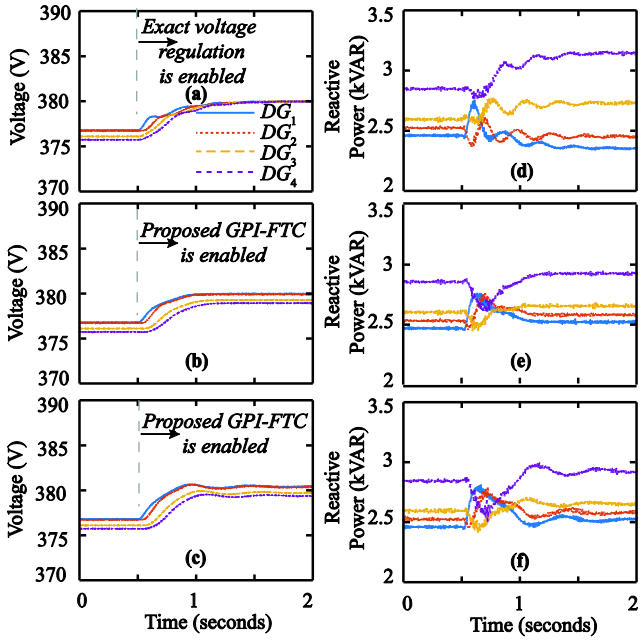

FIGURE 8. DG voltage and reactive power under different control methods: (a) and (d) proposed GPI-FTC with exact voltage regulation; (b) and (e) proposed GPI-FTC with leader-following voltage regulation scheme (DG1 is the leader); (c) and (f) proposed GPI-FTC with average consensus voltage regulation scheme.

Q-sharing control is activated and the compromise between voltage regulation and the Q-sharing is achieved using (29) and (30), as pointed out in Proposition 2 in Section III. Under the proposed GPI-FTC, the voltage of the leader (i.e. DG 1) is set to the reference value and the voltages of the follower DGs are varied with respect to the Q-sharing controlled and line impedances. As shown in Fig. 7 (c), the voltages all the DGs are kept within the practical range. When Load 6 is connected at $t = 4.5s$, it can be seen from Figs. 7 (a) and (b) that the proposed GPI-FTC automatically regulates the frequency and share the new power demand based on the droop gains, automatically. In addition, the voltage profile is regulated under the proposed GPI-FTC.

C. CASE 3. PERFORMANCE COMPARISON OF THE PROPOSED Q-SHARING GPI-FTC WITH EXACT VOLTAGE REGULATION

In this case, the performance of the proposed GPI-FTC is compared with the exact voltage regulation method. The proposed GPI-FTC is enabled at t = 0.5s. Figs (a), (b) and (c) are DG voltage under exact voltage regulation scheme, proposed GPI-FTC with leader-following voltage regulation scheme (DG 1 is the leader), and proposed GPI-FTC with average consensus voltage regulation scheme, while Figs (d), (e) and (f) are their corresponding DG reactive power. The exact voltage regulation as well as the proposed GPI-FTC are enabled at $t = 0.5s$. As depicted in Figs. 8 (a) and (d), the exact voltage regulation method can regulate all voltage of DGs to the nominal voltage (380 V), but it can not realize

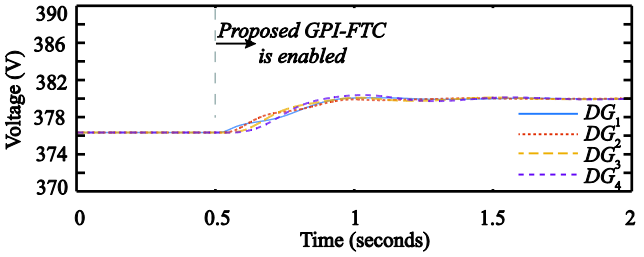

FIGURE 9. Outputs of the distributed average voltage observer.

desirable Q-sharing (Fig. 8 (d))as there is no additional degree of freedom. For the proposed GPI-FTC, either the leader voltage (DG 1 in Fig. 8 (b)) or average voltage (Fig. 8 (c)) is regulated to the nominal voltage and Q-sharing control (Figs. 8 (e) and (f)) can be conducted simultaneously. The outputs of the distributed observer for proposed GPI-FTC with average consensus voltage regulation scheme ((c) and (f) in Fig. 8) are shown in Fig. 9. It can be seen that the distributed observer outputs (i.e. estimated average voltages) of all the DG units converge soon after the proposed GPI-FTC is enabled.

D. CASE 4. SUDDEN OUTAGE OF DG 3

In the following, the performance of the proposed GPI-FTC is examined under converter outage. At the beginning, the microgrid system is under the proposed GPI-FTC, while DG 3 is suddenly disconnected at $t = 0.5s$. The original CN topology before DG 3 outage is depicted in Fig. 5 (a), whereas it is changed to Fig. 5 (b) after DG 3 outage. Performance of the proposed GPI-MDSC in regulating the state variables after sudden outage of DG 3 is shown in Fig. 10. The results in Fig. 10 confirm the resiliency of the proposed GPI-FTC to preserve the stability of the microgrid with diverse configurations of the CN under DG outage.

E. CASE 5: PERFORMANCE COMPARISON OF THE PROPOSED GPI-FTC WITH THE CONVENTIONAL PI CONTROLLER

In this case, the performance of the proposed GPI-FTC is compared with the conventional P-shaped controllers in (37) and (39) and the PI-shaped controllers in (36) and (38). First the impact of the added consensus-based dynamic on performance of the proposed GPI-FTC is evaluated in Fig. 11 and then the proposed GPI-FTC is compared to existing P-shaped and PI-shaped controllers in Fig. 12. The secondary frequency and active power controllers are enabled at $t = 0.5s$.

The control gains are set to $k^P_{\omega,i} = k^P_{P,i} = 15$ and $k^I_{\omega,i} = k^I_{P,i} = 60$ for both the proposed controllers. In order to examine the impact of the proposed consensus-based integrand terms (i.e. $-\mathbf{K}^Z_\omega \mathbf{L}\text{sig}^\alpha(\mathbf{z}_\omega)$ in (24) and $-\mathbf{K}^Z_P \mathbf{L}\text{sig}^\alpha(\mathbf{z}_P)$ in (25)), the gains $k^Z_{\omega,i}$ and $k^Z_{P,i}$ are increased from 4 to 15 in the proposed GPI-DCS, whereas $k^Z_{\omega,i} = k^Z_{P,i} = 0$ in the conventional PI control. Results are shown in Fig 11.

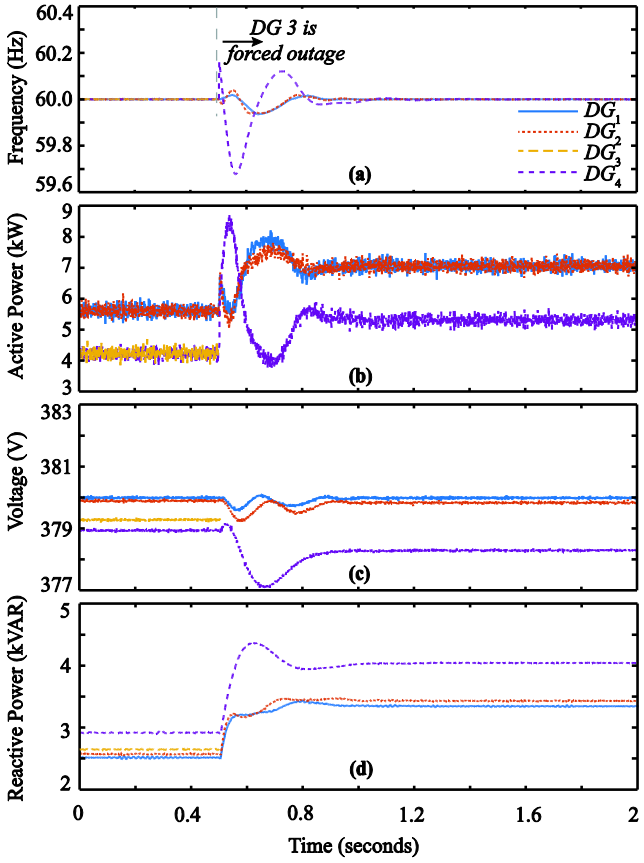

FIGURE 10. **Large signal stability of the proposed controller when DG 3 is forced outage: (a) Frequency; (b) Voltage; (c) Active power; (d) Reactive power.**

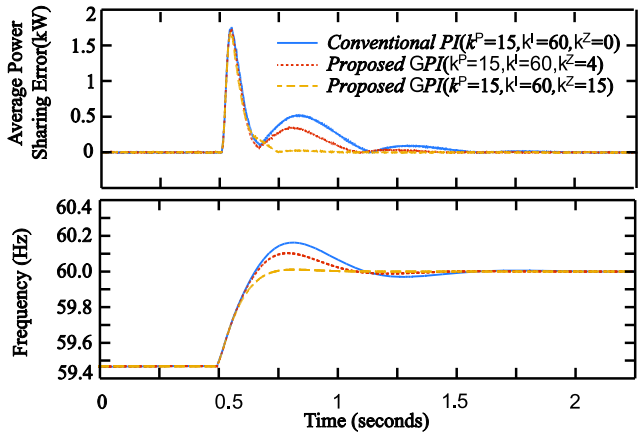

FIGURE 11. **Impact of adding the proposed consensus-based integrand term and Performance comparison of the proposed GPI-DCS with the conventional PI (a) Average power sharing error, (b) Frequency.**

As depicted in Fig. 11, the proposed GPI-FTC improves the transient response of the P-sharing error and the frequency, compared to the conventional PI control, by reducing the overshoot and the settling time. It is also worth noting that with the arbitrary PI gains and by increasing $\gamma_{\omega i}$ and γ_{Pi} from 4 to 15, the overshoot is further decreased, which verifies the

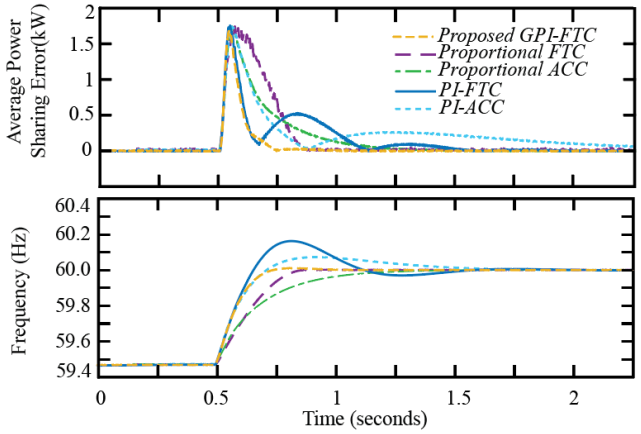

FIGURE 12. **Performance comparison of the proposed GPI-DCS with the conventional P-shaped FTC [22], [24], P-shaped ACC (i.e., not FTC) with asymptotic convergence [6], [16], [17], [29], [R1], [R2], PI-shaped FTC [19], [21], [26], and PI-shaped ACC (i.e., not FTC) [11], [12], [28], [R3], [R4] (a) Average power sharing error, (b) Frequency.**

advantage of adding the proposed consensus-based integrand term to the conventional PI control scheme.

Moreover, the performance of the proposed GPI-FTC is compared to the conventional P-shaped FTC [22], [24], P-shaped ACC (i.e. not FTC) with asymptotic convergence [6], [16], [17], [29], [R1], [R2], PI-shaped FTC [19], [21], [26], and PI-shaped ACC (i.e. not FTC) [11], [12], [28], [R3], [R4] in Fig. 12. It is shown that the transient response of the frequency regulation and power-sharing loops are improved using the proposed GPI-FTC compared to conventional control schemes.

V. CONCLUSION

This paper proposed a generalized proportional-integral controller for distributed secondary regulation of frequency and voltage and power-sharing in a standalone microgrid. The conventional proportional and PI controllers with asymptotic and finite-time convergence can be modelled as specific case of the proposed GPI-FTC under specific parameter settings. The proposed GPI-FTC is synthesized by modifying the traditional PI scheme and adding a consensus term to the integrand dynamics. The proposed GPI-FTC improves the transient response of the traditional distributed PI schemes and provides fast and finite-time convergence of the system states. The control actions are determined by communicating to neighbor units, which enables scalability and supports plug-n-play features. Stability and design of the presented GPI-FTC follows the control Lyapunov function technique. Lyapunov stability and finite-time convergence of the control loops are proved mathematically and their performance are evaluated through numerical studies employing detailed switched models of the microgrid. Firstly, the result of small signal analysis confirms that the proposed GPI-FTC improves the transient and steady state response of the control loop. The performance of the proposed GPI-FTC is verified under load

change and sudden DG outage. The Q-sharing in the proposed GPI-FTC is compared with the exact and average voltage regulation. Transient performance of the proposed GPI-FTC is compared to conventional PI controllers and it superiority is shown.

REFERENCES

[1] D. E. Olivares *et al.*, "Trends in microgrid control," *IEEE Trans. Smart Grid*, vol. 5, no. 4, pp. 1905–1919, Jul. 2014.

[2] J. M. Guerrero, J. C. Vasquez, J. Matas, L. G. D. Vicuña, and M. Castilla, "Hierarchical control of droop-controlled AC and DC microgrids—A general approach towards standardization," *IEEE Trans. Ind. Electron.*, vol. 58, no. 1, pp. 158–172, Jan. 2011.

[3] M. Yazdanian and A. Mehrizi-Sani, "Distributed control techniques in microgrids," *IEEE Trans. Smart Grid*, vol. 5, no. 6, pp. 2901–2909, Nov. 2014.

[4] J. M. Guerrero, M. Chandorkar, T.-L. Lee, and P. C. Loh, "Advanced control architectures for intelligent microgrids—Part I: Decentralized and hierarchical control," *IEEE Trans. Ind. Electron.*, vol. 60, no. 4, pp. 1254–1262, Apr. 2013.

[5] Y. Khayat *et al.*, "On the secondary control architectures of AC microgrids: An overview," *IEEE Trans. Power Electron.*, vol. 35, no. 6, pp. 6482–6500, Jun. 2020.

[6] Q. Zhou, M. Shahidehpour, A. Paaso, S. Bahramirad, A. Alabdulwahab, and A. Abusorrah, "Distributed control and communication strategies in networked microgrids," *IEEE Commun. Surveys Tuts.*, vol. 22, no. 4, pp. 2586–2633, 4th Quart., 2020.

[7] Q. Li, F. Chen, M. Chen, J. M. Guerrero, and D. Abbott, "Agent-based decentralized control method for islanded microgrids," *IEEE Trans. Smart Grid*, vol. 7, no. 2, pp. 637–649, Mar. 2016.

[8] A. H. Etemadi, E. J. Davison, and R. Iravani, "A generalized decentralized robust control of islanded microgrids," *IEEE Trans. Power Syst.*, vol. 29, no. 6, pp. 3102–3113, Nov. 2014.

[9] A. H. Etemadi, E. J. Davison, and R. Iravani, "A decentralized robust control strategy for multi-DER microgrids—Part I: Fundamental concepts," *IEEE Trans. Power Del.*, vol. 27, no. 4, pp. 1843–1853, Oct. 2012.

[10] W. Liu, W. Gu, W. Sheng, X. Meng, Z. Wu, and W. Chen, "Decentralized multi-agent system-based cooperative frequency control for autonomous microgrids with communication constraints," *IEEE Trans. Sustain. Energy*, vol. 5, no. 2, pp. 446–456, Apr. 2014.

[11] A. Bidram, A. Davoudi, F. L. Lewis, and J. M. Guerrero, "Distributed cooperative secondary control of microgrids using feedback linearization," *IEEE Trans. Power Syst.*, vol. 28, no. 3, pp. 3462–3470, Aug. 2013.

[12] B. Abdolmaleki, Q. Shafiee, A. R. Seifi, M. M. Arefi, and F. Blaabjerg, "A zeno-free event-triggered secondary control for AC microgrids," *IEEE Trans. Smart Grid*, vol. 11, no. 3, pp. 1905–1916, May 2020, doi: 10.1109/TSG.2019.2945250.

[13] S. T. Cady, A. D. Dominguez-Garcia, and C. N. Hadjicostis, "A distributed generation control architecture for islanded AC microgrids," *IEEE Trans. Control Syst. Technol.*, vol. 23, no. 5, pp. 1717–1735, Sep. 2015.

[14] G. Lou, W. Gu, J. Wang, W. Sheng, and L. Sun, "Optimal design for distributed secondary voltage control in islanded microgrids: Communication topology and controller," *IEEE Trans. Power Syst.*, vol. 34, no. 2, pp. 968–981, Mar. 2019.

[15] Q. Li, C. Peng, M. Wang, M. Chen, J. M. Guerrero, and D. Abbott, "Distributed secondary control and management of islanded microgrids via dynamic weights," *IEEE Trans. Smart Grid*, vol. 10, no. 2, pp. 2196–2207, Mar. 2019.

[16] X. Lu, X. Yu, J. Lai, J. M. Guerrero, and H. Zhou, "Distributed secondary voltage and frequency control for islanded microgrids with uncertain communication links," *IEEE Trans. Ind. Informat.*, vol. 13, no. 2, pp. 448–460, Apr. 2017.

[17] N. M. Dehkordi, N. Sadati, and M. Hamzeh, "Fully distributed cooperative secondary frequency and voltage control of islanded microgrids," *IEEE Trans. Energy Convers.*, vol. 32, no. 2, pp. 675–685, Jun. 2017.

[18] A. Bidram, A. Davoudi, and F. L. Lewis, "Finite-time frequency synchronization in microgrids," in *Proc. IEEE Energy Convers. Congr. Expo. (ECCE)*, Sep. 2014, pp. 4305–4310.

[19] S. Zuo, A. Davoudi, Y. Song, and F. L. Lewis, "Distributed finite-time voltage and frequency restoration in islanded AC microgrids," *IEEE Trans. Ind. Electron.*, vol. 63, no. 10, pp. 5988–5997, Oct. 2016.

[20] Q. Zhou, M. Shahidehpour, M. Yan, X. Wu, A. Alabdulwahab, and A. Abusorrah, "Distributed secondary control for islanded microgrids with mobile emergency resources," *IEEE Trans. Power Syst.*, vol. 35, no. 2, pp. 1389–1399, Mar. 2020.

[21] X. Lu, X. Yu, J. Lai, Y. Wang, and J. M. Guerrero, "A novel distributed secondary coordination control approach for islanded microgrids," *IEEE Trans. Smart Grid*, vol. 9, no. 4, pp. 2726–2740, Jul. 2018.

[22] A. M. Shotorbani, S. G. Zadeh, B. Mohammadi-Ivatloo, and S. H. Hosseini, "A distributed non-Lipschitz control framework for self-organizing microgrids with uncooperative and renewable generations," *Int. J. Electr. Power Energy Syst.*, vol. 90, pp. 267–279, Sep. 2017.

[23] A. M. Shotorbani, S. Ghassem-Zadeh, B. Mohammadi-Ivatloo, and S. H. Hosseini, "A distributed secondary scheme with terminal sliding mode controller for energy storages in an islanded microgrid," *Int. J. Electr. Power Energy Syst.*, vol. 93, pp. 352–364, Dec. 2017.

[24] Z. Deng, Y. Xu, H. Sun, and X. Shen, "Distributed, bounded and finite-time convergence secondary frequency control in an autonomous microgrid," *IEEE Trans. Smart Grid*, vol. 10, no. 3, pp. 2776–2788, May 2019.

[25] Y. Xu, H. Sun, W. Gu, Y. Xu, and Z. Li, "Optimal distributed control for secondary frequency and voltage regulation in an islanded microgrid," *IEEE Trans. Ind. Informat.*, vol. 15, no. 1, pp. 225–235, Jan. 2019.

[26] N. M. Dehkordi, N. Sadati, and M. Hamzeh, "Distributed robust finite-time secondary voltage and frequency control of islanded microgrids," *IEEE Trans. Power Syst.*, vol. 32, no. 5, pp. 3648–3659, Sep. 2017.

[27] Q. Shafiee, V. Nasirian, J. C. Vasquez, J. M. Guerrero, and A. Davoudi, "A multi-functional fully distributed control framework for AC microgrids," *IEEE Trans. Smart Grid*, vol. 9, no. 4, pp. 3247–3258, Jul. 2018.

[28] Q. Shafiee, J. M. Guerrero, and J. C. Vasquez, "Distributed secondary control for islanded microgrids—A novel approach," *IEEE Trans. Power Electron.*, vol. 29, no. 2, pp. 1018–1031, Feb. 2014.

[29] A. Bidram, A. Davoudi, F. L. Lewis, and Z. Qu, "Secondary control of microgrids based on distributed cooperative control of multi-agent systems," *IET Generat., Transmiss., Distrib.*, vol. 7, no. 8, pp. 822–831, Aug. 2013.

[30] X. Wang, S. Li, and P. Shi, "Distributed finite-time containment control for double-integrator multiagent systems," *IEEE Trans. Cybern.*, vol. 44, no. 9, pp. 1518–1528, Sep. 2014.

[31] W. M. Haddad and A. L'Afflitto, "Finite-time stabilization and optimal feedback control," *IEEE Trans. Autom. Control*, vol. 61, no. 4, pp. 1069–1074, Apr. 2016.

[32] J. W. Simpson-Porco, Q. Shafiee, F. Dorfler, J. C. Vasquez, J. M. Guerrero, and F. Bullo, "Secondary frequency and voltage control of islanded microgrids via distributed averaging," *IEEE Trans. Ind. Electron.*, vol. 62, no. 11, pp. 7025–7038, Nov. 2015.

[33] J. Lai, H. Zhou, X. Lu, X. Yu, and W. Hu, "Droop-based distributed cooperative control for microgrids with time-varying delays," *IEEE Trans. Smart Grid*, vol. 7, no. 4, pp. 1775–1789, Jul. 2016.

[34] Q. Shafiee, C. Stefanovic, T. Dragicevic, P. Popovski, J. C. Vasquez, and J. M. Guerrero, "Robust networked control scheme for distributed secondary control of islanded microgrids," *IEEE Trans. Ind. Electron.*, vol. 61, no. 10, pp. 5363–5374, Oct. 2014.

[35] A. Bidram, A. Davoudi, and F. L. Lewis, "A multiobjective distributed control framework for islanded AC microgrids," *IEEE Trans. Ind. Informat.*, vol. 10, no. 3, pp. 1785–1798, Aug. 2014.

YUANSHI ZHANG (Student Member, IEEE) received the B.Eng. and M.A.Sc. degrees from the Harbin Institute of Technology, China, in 2013 and 2015, respectively. He is currently pursuing the Ph.D. degree with The University of British Columbia Okanagan, Canada. His current research interests include power system analysis, and modeling and control of modular-multilevel-converter-based high-voltage direct current transmission systems.

AMIN MOHAMMADPOUR SHOTORBANI (Member, IEEE) received the Ph.D. degree in electrical engineering from the University of Tabriz, Iran, in 2017. He was a Post-Doctoral Research Fellow with the University of Tabriz from 2017 to 2018. He has been a Post-Doctoral Research Fellow with The University of British Columbia Okanagan, Kelowna, BC, Canada, since July 2018. His research interests include nonlinear and distributed controls, power system stability, intelligent energy systems, microgrids, and renewables integration.

LIWEI WANG (Member, IEEE) received the Ph.D. degree in electrical engineering from The University of British Columbia, Vancouver, BC, Canada, in 2010. He worked with ABB Corporate Research, Sweden, as a Senior Scientist. In 2014, he joined the School of Engineering, The University of British Columbia Okanagan, Kelowna, BC, Canada, as an Assistant Professor. His research interests include power systems, electrical machines and drives, utility power electronics, and distributed generation.

BEHNAM MOHAMMADI-IVATLOO (Senior Member, IEEE) received the M.Sc. and Ph.D. degrees in electrical engineering from the Sharif University of Technology, Tehran, Iran. He is currently a Professor with the University of Tabriz, Tabriz, Iran, where he is also the Head of the Smart Energy Systems Laboratory. Before joining the University of Tabriz, he was a Research Associate with the Institute for Sustainable Energy, Environment and Economy, University of Calgary, Canada. He has a mix of high-level experience in research, teaching, and administration and voluntary jobs at the national and international levels. He was a PI or a Co-PI in 20 externally funded research projects. He is included in the 2018 and 2019 Thomson Reuters' list of the top 1% most cited researchers. His research interests include integrated energy systems, renewable energies, microgrid systems, and smart grids. He has been a member of the Governing Board of Iran Energy Association since 2013, where he was elected as the President in 2019. He is also serving as an Editor or an Associate Editor for different journals, such as IEEE TRANSACTIONS ON POWER SYSTEMS, IEEE ACCESS, *IET Smart Grid*, and *Sustainability*.